Solid State Ionics 333 (2019) 1–8

Contents lists available at ScienceDirect

Solid State Ionics

journal homepage: www.elsevier.com/locate/ssi

Understanding the effect of Ce and Zr on chemical expansion in yttrium doped strontium cerate and zirconate by high temperature X-ray analysis and density functional theory

Takaya Fujisaki[a,*], Aleksandar Tsekov Staykov[b], Yuhang Jing[c], Kwati Leonard[b], Narayana R. Aluru[c], Hiroshige Matsumoto[b,d,**]

[a] Molecular and Material Science, Interdisciplinary Graduate School of Engineering Sciences, Kyushu University, 744 Motooka, Nishi-Ku, Fukuoka 819-0395, Japan
[b] International Institute for Carbon-Neutral Energy Research (WPI-I2CNER), Kyushu University, 744 Motooka, Nishi-Ku, Fukuoka 819-0395, Japan
[c] Department of Mechanical Science and Engineering, University of Illinois at Urbana–Champaign, Urbana, IL 61801, United States
[d] Next-Generation Fuel Cell Research Center (Next-FC), Kyushu University, 744 Motooka, Nishi-Ku, Fukuoka 819-0395, Japan

ARTICLE INFO

Keywords:
Perovskite
Proton conductor
High temperature X-ray analysis
Thermogravimetric analysis
Density functional theory

ABSTRACT

Aliovalent cation-doped perovskite-type oxides (ABO_3) exhibit proton conductivity originating from the hydration of oxide ion vacancies, which is accompanied by structural deformation, i.e. chemical expansion. The chemical expansion may lead to failure in electrochemical devices, and thus it is necessary to understand the causes of this process at the atomic scale. In this study, the chemical expansion behaviors of Y-doped strontium cerate and zirconate were comparatively investigated. High-temperature X-ray diffraction (HT-XRD) and thermogravimetric analysis (TGA) revealed that the cerate exhibits larger chemical expansion. Density Functional Theory (DFT) calculations revealed that this tendency can be accounted for by the different atomic distribution of the Y dopant between the cerate and zirconate, which results in differences in the size of the oxide ion vacancies to be hydrated as well as different elastic character.

1. Introduction

To reduce the use of fossil fuels, one possible approach is to improve the energy conversion efficiencies of alternative energy technologies. Solid oxide fuel cells (SOFCs) are promising energy conversion devices characterized by energy conversion efficiencies higher than those of conventional thermal power systems. Another approach is to utilize renewable energy sources, i.e., solar energy, wind energy, etc., or the combination of fuel cells and water electrolysis which will allow mass energy storage via hydrogen storing techniques [1–3]. Solid oxide fuel cells and solid oxide electrolysis cells (SOECs) have higher energy conversion efficiencies than low-temperature fuel cells and water electrolyzers. Therefore, solid oxide cells are promising candidates for reducing the reliance on fossil fuel energy.

The operating temperatures of the current SOFCs and SOECs, which primarily use stabilized zirconia as the electrolyte, are higher than 700 °C. Such high temperatures are necessary to ensure sufficient mobility of the oxide ions in the solid oxide electrolytes, as well as fast kinetics at the electrodes. However, the high operating temperatures require the use of high-cost materials and result in the degradation of cell performance over time. Thus, lowering the operating temperature is an important challenge underlying the development of solid oxide cells.

Proton-conducting oxides based on aliovalent-doped perovskites have attracted attention because proton conduction proceeds in temperature ranges lower than those required by oxide ion-conductor-based oxide cells [4] due to the relatively low temperature dependence of proton mobility in comparison with that of oxide ion mobility. Formation of the protonic charge carriers is commonly understood to proceed via the hydration of oxide ion vacancies:

$$H_2O + V_o^{\cdot\cdot} \rightleftarrows O_o^{\times} + 2H_i^{\cdot} \quad (1)$$

where $V_o^{\cdot\cdot}$, $O_o^{\times}$, and $H_i^{\cdot}$ denote oxide-ion vacancy, oxide ion at its regular site, and proton, respectively, in Kröger-Vink notation [5,6]. Thus, hydration is the key process allowing proton conduction to take place in the oxides. However, a side effect of this hydration is chemical

* Corresponding author.
** Correspondence to: H. Matsumoto, International Institute for Carbon-Neutral Energy Research (I2CNER), Kyushu University, 744 Motooka, Nishi-ku (Buiding II, Room 303), Fukuoka 819-0395, Japan.
E-mail addresses: takaya.fujisaki.328@s.kyushu-u.ac.jp (T. Fujisaki), matsumoto@i2cner.kyushu-u.ac.jp (H. Matsumoto).

https://doi.org/10.1016/j.ssi.2019.01.009
Received 24 October 2018; Received in revised form 28 December 2018; Accepted 7 January 2019

expansion; the incorporation of a water molecule into an oxide vacancy results in expansion of the perovskite lattice, leading to possible damage to the solid oxide cell components induced by mismatches in the dimensions of the proton conducting oxides, electrodes, and gas seals [7]. To reduce such chemical expansion, its cause must first be clarified, and then a suitable chemical composition must be designed so as to minimize the expansion coefficient [7]. This study employs strontium cerate and strontium zirconate as two model materials to assess how the incorporation of cerium or zirconium at the *B*-site of ABO_3 differentially affects the hydration-induced chemical expansion. The use barium at the *A*-site is beneficial for obtaining high conductivity, although barium can be volatilized at high temperatures. For simplicity, strontium was selected as the *A*-site cation in this study. Yttrium was chosen as a typical dopant for the *B*-site, which works to provide oxide ion vacancies for hydration.

Computational science has been enthusiastically employed to theoretically evaluate properties of ion conducting solids [8,9]. Because experimental approach is limited to investigate atomic scale properties of proton conducting oxides, Density Functional Theory (DFT) for first-principle simulations has been recognized as being beneficial approach. As an example of computational approach for proton conducting oxides, Jing et al. investigated the hydration enthalpies of proton conducting oxides can be negative after hydration process [10]. In this study, DFT is employed to investigate the influence of Ce and Zr at the *B*-site on chemical expansion in the proton conducting oxides. High-temperature X-ray diffraction (HT-XRD) and thermogravimetric analysis (TGA) were employed to experimentally evaluate the degree of hydration and chemical expansion in the two proton-conducting oxides.

2. Experimental

2.1. Experimental procedure

2.1.1. Material preparation

Ceramic powders equivalent to the chemical compositions of $SrCe_{0.922}Y_{0.078}O_{3-\delta}$ and $SrZr_{0.922}Y_{0.078}O_{3-\delta}$ were prepared by a solid state reaction method previously described [11,12]. Powders of $SrCO_3$, CeO_2, ZrO_2, and Y_2O_3 were used as starting materials. The powders were weighed appropriately, mixed, and calcined for 10 h in air at 1250 °C for yttrium-doped strontium cerate and at 1350 °C for yttrium-doped strontium zirconate. The products were ground with a planetary ball mill, isostatically pressed into disk shapes at 250 MPa, and sintered for 10 h to obtain dense ceramics. Sintering temperatures were 1550 °C for yttrium-doped strontium cerate and 1650 °C for yttrium-doped strontium zirconate. Finally, $SrCe_{0.922}Y_{0.078}O_{3-\delta}$ and $SrZr_{0.922}Y_{0.078}O_{3-\delta}$ powders were obtained by grinding sintered pellets into granules. X-ray diffraction (XRD) measurements were taken at room temperature using a Rigaku Ultima IV diffractometer with Cu Kα irradiation (40 kV, 40 mA) to confirm that the diffraction patterns of the prepared materials agreed with the perovskite structure of $SrCeO_3$ (ICSD 01-083-1157) and $SrZrO_3$ (ICSD 00-044-0161), with no secondary phases.

2.1.2. High temperature X-ray analysis

HT-XRD analyses were carried out in the temperature range between 100 °C and 1200 °C in a humidified nitrogen gas stream ($p(H_2O)$ = 1.9 kPa) to investigate the chemical expansion behavior of $SrCe_{0.922}Y_{0.078}O_{3-\delta}$ and $SrZr_{0.922}Y_{0.078}O_{3-\delta}$. First, the temperature was maintained at 50 °C for 60 min and then increased to 1200 °C at a heating rate of 60 °C/min. After holding at 1200 °C for 180 min, the temperature was decreased from 1200 °C to 100 °C and XRD patterns were obtained every 100 °C. The cooling rates were 20 °C/min from 1200 to 500 °C, 10 °C/min from 500 to 400 °C, 5 °C/min from 400 to 300 °C, and 2 °C/min from 300 to 100 °C, and the measurements were taken every 10 min (1200–600 °C), 20 min (500–400 °C), or 30 min (300–100 °C). Each volume constant was obtained every 100 °C after the change was stabilized sufficiently.

2.1.3. Thermogravimetric analysis

TGA (TG-DSC, NETZSCH Jupiter, STA449F3) was carried out to evaluate the amount of water incorporated in the proton conductor specimens. The granular samples were heated from 50 °C to 1200 °C at 5 °C/min in dry N_2 and kept at 1200 °C for 90 min. Then, the dry N_2 atmosphere was changed to wet N_2 ($p(H_2O)$ = 950 Pa or 633 Pa) and cooled to 100 °C. During cooling, the temperature was decreased in 100 °C increments and maintained at each 100 °C step for 60 min.

2.2. Computational details

All DFT calculations were performed using the Vienna Ab initio simulation package (VASP) [13–15]. The Perdew-Burke-Ernzerhof (PBE) [16] exchange-correlation functional was employed based on the projector-augmented wave (PAW) method [13]. The cutoff energy for the plane wave basis set was 500 eV for all calculations. A DFT + U approach was applied to the f-orbitals of Ce with a value of U = 5 eV [17]. The PAW method pseudopotentials with valence states of Sr (4s, 4p, 5s, 4d), Zr (4s, 4p, 5s, 4d), Ce (5s, 5p, 5d, 4f, 6s), Y (4s, 4p, 5s, 4d), and O (2s, 2p) were used for all calculations. All ionic positions were optimized by a conjugate gradient method until the forces on each ion were below 10^{-2} eV/Å^2. Electronic energy was converged to 10^{-4} eV and ion positions were converged to forces of 10^{-2} eV/Å^2. Cell parameters were converged to stress of 10^{-2} eV/Å. Lower criteria for electronic energy conversion would yield in forces with lower accuracy which should not allow us to complete correcting the cell parameters and thus, the chemical expansion was evaluated. In addition, we have performed spin polarized calculations as shown in Fig. S1. However, there is no difference in the density of state between spin up and spin down levels. That is why we have chosen spin unpolarized calculations for our study.

The computed lattice parameters were consistent with those determined experimentally and by DFT calculations in previous reports, as shown in Table 1 [18–20]. On the basis of the optimized unit cell, $SrZrO_3$ and $SrCeO_3$ supercells with $2 \times 2 \times 2$ orthorhombic $Sr_{32}Zr_{32}O_{96}$ and $2 \times 2 \times 2$ orthorhombic $Sr_{32}Ce_{32}O_{96}$ cells were constructed and optimized using $3 \times 3 \times 4$ and $3 \times 3 \times 4$ Monkhorst-Pack *k*-points meshes, respectively. Further, one oxide ion vacancy was introduced by substituting two Y for Ce or Zr, creating $Sr_{32}Zr_{30}Y_2O_{95}$ and $Sr_{32}Ce_{32}Y_2O_{95}$, respectively. Their all models are in bulk dimension. Hydrated $Sr_{32}Zr_{30}Y_2O_{95}$ and $Sr_{32}Ce_{32}Y_2O_{95}$ supercells, whose respective compositions are described as $Sr_{32}Zr_{30}Y_2O_{96}H_2$ and $Sr_{32}Ce_{30}Y_2O_{96}H_2$, were also optimized. To evaluate the chemical expansion of either composition, the lattice volumes of $Sr_{32}Zr_{30}Y_2O_{95}$, $Sr_{32}Ce_{30}Y_2O_{95}$, $Sr_{32}Zr_{30}Y_2O_{96}H_2$, and $Sr_{32}Ce_{30}Y_2O_{96}H_2$ were estimated.

3. Results and discussion

3.1. Chemical expansion determined by HT-XRD

In XRD patterns of $SrCe_{0.922}Y_{0.078}O_{3-\delta}$ and $SrZr_{0.922}Y_{0.078}O_{3-\delta}$ measured at the respective temperatures under a wet N_2 atmosphere (p

Table 1
Calculated and experimental lattice parameters of $SrZrO_3$ and $SrCeO_3$.

Solid oxide	Lattice parameter	This work, GGA-PBE	GGA-PBE	Experiment
$SrZrO_3$ (orthorhombic)	a (Å)	5.70	5.81[18]	5.79[19]
	b (Å)	5.74	5.87[18]	5.82[19]
	c (Å)	8.19	8.24[18]	8.20[19]
$SrCeO_3$ (orthorhombic)	a (Å)	6.07	5.945[20]	6.01[20]
	b (Å)	6.24	6.103[20]	6.15[20]
	c (Å)	8.70	8.506[20]	8.60[20]

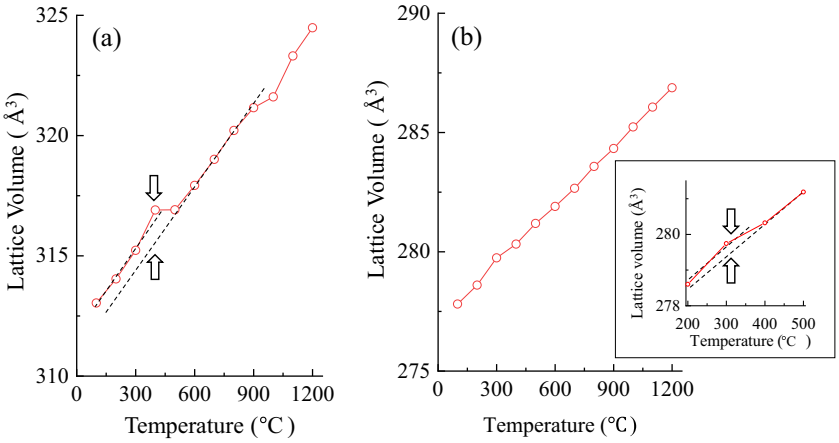

Fig. 1. Temperature dependence of lattice volumes of $SrCe_{0.922}Y_{0.078}O_{3-\delta}$ (a) and $SrZr_{0.922}Y_{0.078}O_{3-\delta}$ (b).

(H_2O) = 1.9 kPa) (Fig. S2a and b), diffraction peaks shifted to lower angles with increasing temperature, indicating that the lattices expanded as temperature increased. Fig. 1(a) and (b) are the results of evaluating the lattice volume from 1200 °C to 100 °C in wet N_2 atmosphere ($p(H_2O)$ = 1.9 kPa). Each plot is the lattice volume measured every 100 °C. A discontinuous change in the lattice volume is observed at around 400–600 °C due to chemical expansion originating from hydration of the oxide vacancies, as shown by dashed lines in Fig. 1(a) and (b). Although the chemical expansion of $SrZr_{0.922}Y_{0.078}O_{3-\delta}$ is much smaller than $SrCe_{0.922}Y_{0.078}O_{3-\delta}$, it is recognized in enlarged inset in Fig. 1(b). Chemical expansion by volume is defined as the ratio of $\Delta V_{lattice}$, the discontinuous change in the lattice volume, to the unit cell volume of un-hydrated perovskite lattice, $V_{lattice}$, as summarized by the following equation:

$$(\text{Chemical expansion}) = \Delta V_{lattice}/V_{lattice} \quad (2)$$

This ratio corresponds to the difference between the cell volumes of the hydrated and un-hydrated forms. As summarized in Table 2, the chemical expansions were determined to be 0.0030 (0.30%) and 0.0016 (0.16%) for $SrCe_{0.922}Y_{0.078}O_{3-\delta}$ and $SrZr_{0.922}Y_{0.078}O_{3-\delta}$, respectively.

3.2. Thermogravimetric analysis (TGA)

TGA was conducted for $SrCe_{0.922}Y_{0.078}O_{3-\delta}$ and $SrZr_{0.922}Y_{0.078}O_{3-\delta}$ to evaluate their proton concentrations. The weight changes were estimated based on increases in the sample weight relative to the weight in dry N_2 at 1200 °C, assuming that the specimens were almost completely dehydrated at this temperature, and the weight change was converted to the degree of hydration based on the reaction shown in Eq. (1). As seen in Fig. 2, the weight change during the heating process was larger than that during the cooling process. This is presumably due to the influence of the physical adsorption of water on the sample surface before starting the measurement, and thus the amount of hydration was evaluated from the data obtained during the cooling process. The degree of hydration is defined by the following equation.

$$(\text{Degree of hydration}) = [OH]/[Y] \quad (3)$$

where [OH] and [Y] are the molar amounts of protons and yttrium relative to the molar amount of the mother ABO_3 perovskite. As shown in Table 2, the degree of hydration of $SrCe_{0.922}Y_{0.078}O_{3-\delta}$ in wet N_2 ($p(H_2O)$ = 633 Pa and 950 Pa), 0.20–0.24, was smaller than that of $SrZr_{0.922}Y_{0.078}O_{3-\delta}$, 0.50–0.53. The degree of hydration was not significantly dependent on the humidity in the gas atmosphere, and thus the result can be compared to the chemical expansion data obtained by HT-XRD (under N_2 at 1.9 kPa $p(H_2O)$) described in the former section. Using the data from the HT-XRD and TGA, the chemical expansion coefficient, β_{chem}, can be obtained according to the following equation:

$$\beta_{chem} = (\Delta V_{lattice}/V_{lattice})/[OH] \quad (4)$$

This data is summarized in Table 2. The existence of a linear relation between chemical expansion and hydration is not guaranteed. However, the chemical expansion values cannot be compared without being normalized based on the degree of hydration, and thus β_{chem} is used hereafter for this comparison. The β_{chem} of $SrCe_{0.922}Y_{0.078}O_{3-\delta}$ was approximately 4 times higher than that of $SrZr_{0.922}Y_{0.078}O_{3-\delta}$. It was thus concluded that the choice of using Ce instead of Zr results in greater chemical expansion.

3.3. Chemical expansion evaluated by Density Functional Theory (DFT) first principle simulation

Geometry optimization was carried out for the hydrated and dehydrated yttrium-doped strontium cerate and zirconate supercells by means of DFT simulations. Two Y atoms were introduced in the 2 × 2 × 2 supercells to introduce one oxide ion vacancy or one water molecule, as shown in Fig. 3. The following points lie arbitrarily on the atomic arrangement in the supercells:

(i) Relative locations of the two Y atoms
(ii) Location of the oxide-ion vacancy relative to Y atoms
(iii) Location of protons relative to Y atoms

Table 2
Chemical expansion, degree of hydration, and chemical expansion coefficient of $SrCe_{0.922}Y_{0.078}O_{3-\delta}$ and $SrZr_{0.922}Y_{0.078}O_{3-\delta}$ determined by HT-XRD and TG analysis.

	Chemical expansion[a]	Degree of hydration[b]	Protonic defect concentration	Chemical expansion coefficient: β_{chem}
	$\Delta V_{lattice}/V_{lattice}$	[OH] / [Y]	[OH] (mol/mol)	$(\Delta V_{lattice}/V_{lattice})$ / [OH]
$SrCe_{0.922}Y_{0.078}O_{3-\delta}$	0.0030	0.20–0.24	0.016–0.019	0.16–0.19
$SrZr_{0.922}Y_{0.078}O_{3-\delta}$	0.0016	0.50–0.52	0.039–0.040	0.040–0.041

[a] Determined by HT-XRD at $p(H_2O)$ = 1900 Pa.
[b] Determined by TGA at $p(H_2O)$ = 633 Pa and 950 Pa.

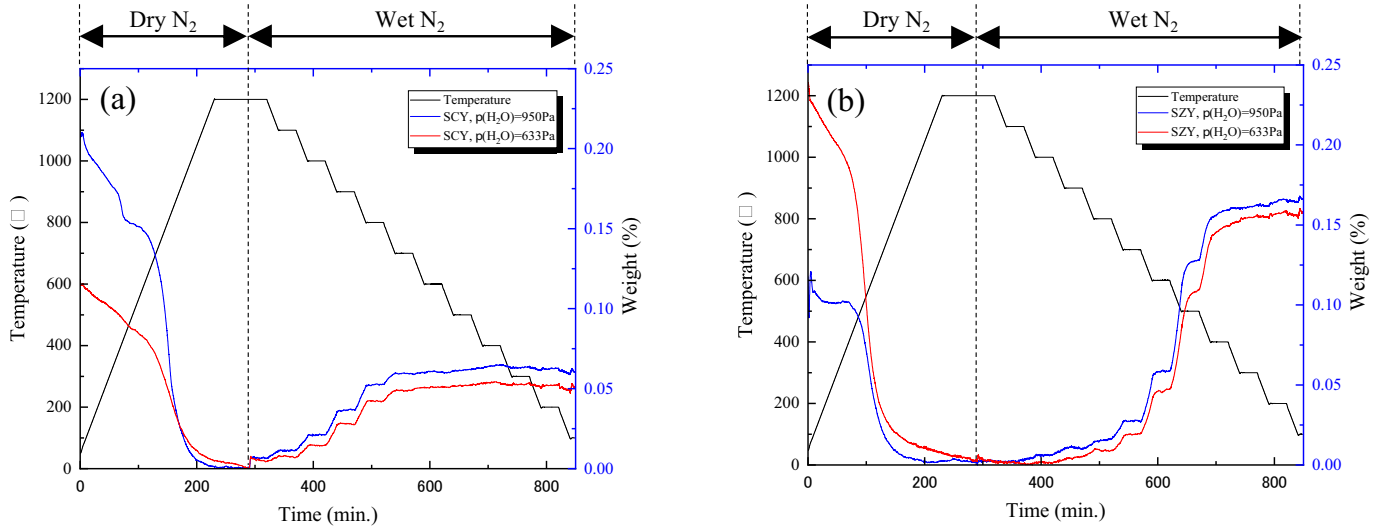

Fig. 2. (Color online) The results of thermogravimetric analysis for $SrCe_{0.922}Y_{0.078}O_{3-\delta}$ (a) and $SrZr_{0.922}Y_{0.078}O_{3-\delta}$ (b) in respective water partial pressure. (For interpretation of the references to color in this figure legend, the reader is referred to the web version of this article.)

As shown later, Y-O-Y clustering results in a more energetically stable state than the case in which the two Y atoms are distant from each other. However, considering the real materials and their preparation processes, since the mobility of Y is relatively low, Y atoms may adopt relatively flexible configurations due to the high-temperature sintering process and the successive cooling period. Similar random positioning of Y dopants has been previously reported, and will be discussed in succeeding sections [21,22]. Therefore, two cases were examined: when the two Y atoms were in closest proximity, linked via one oxygen atom (Fig. 3(a1) and (b1)), and when they were furthest apart (Fig. 3(a2) and (b2)). In regards to points (ii) and (iii) of the list above, oxide ion vacancies and protons have relatively high mobilities, and thus the most energetically stable configurations were employed.

Table 3 shows the enthalpies of $Sr_{32}M_{30}Y_2O_{95}$ (M = Ce or Zr) containing one oxide ion vacancy per supercell (hereafter referred to as $E(Sr_{32}M_{30}Y_2O_{95})$), of one water molecule $E_M(H_2O)$, and of $Sr_{32}M_{30}Y_2O_{96}H_2$ (M = Ce or Zr) $E(Sr_{32}M_{30}Y_2O_{96}H_2)$, in the case wherein the two Y atoms were closest/furthest to each other. $E(Sr_{32}M_{30}Y_2O_{95}H_2)$ was lower than $E(Sr_{32}M_{30}Y_2O_{95}) + E(H_2O)$ in both Y distribution cases, as shown in columns d in Table 3. This implies that

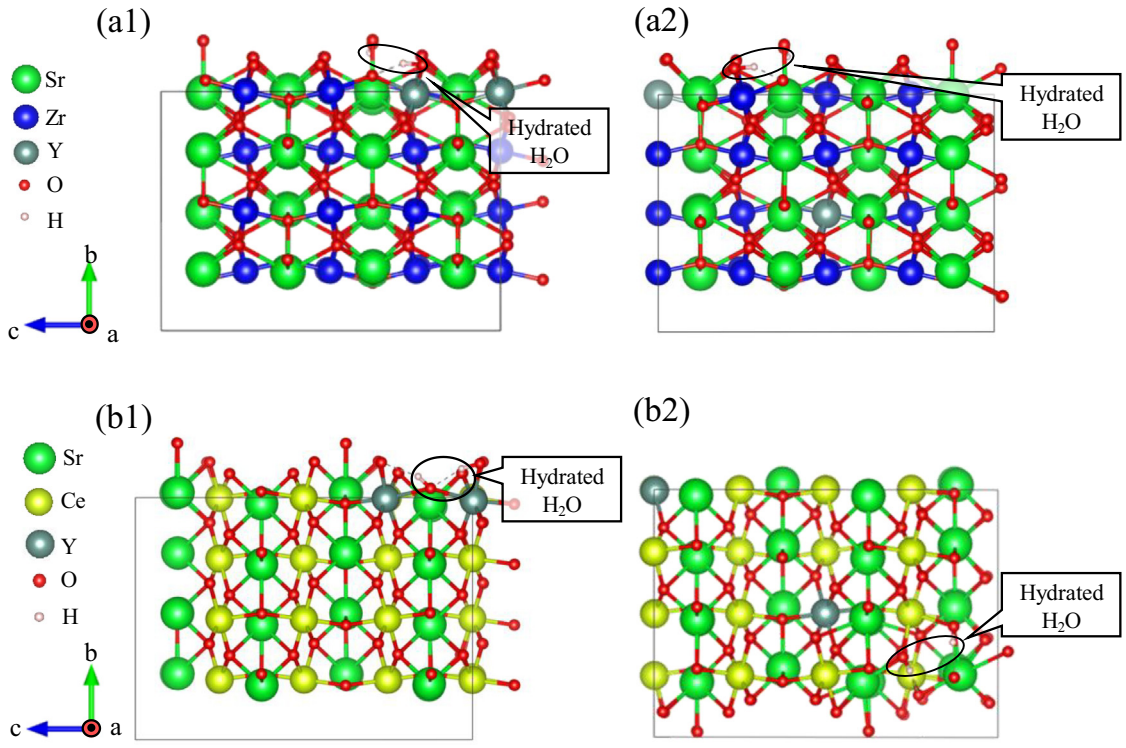

Fig. 3. (Color online) Optimized hydrated yttrium doped strontium cerate (a) and zirconate (b) supercell depending on Y configuration: Y atoms are close each other in $Sr_{32}Zr_{30}Y_2O_{96}H_2$ (a1), Y atoms are distant each other in $Sr_{32}Zr_{30}Y_2O_{96}H_2$ (a2), Y atoms are close each other in $Sr_{32}Ce_{30}Y_2O_{96}H_2$ (b1), and Y atoms are distant each other in $Sr_{32}Ce_{30}Y_2O_{96}H_2$ (b2). Three atoms in black circles are hydrated water molecules. All schematic models are visualized with VESTA [26]. (For interpretation of the references to color in this figure legend, the reader is referred to the web version of this article.)

Table 3
Enthalpies of dehydrated/hydrated yttrium doped strontium cerate/zirconate depending on the Y configuration: The case that Y atoms are close each other and the case that Y atoms are distant each other, and one water molecule. Each water molecule has same lattice volume of dehydrated yttrium doped strontium cerate/zirconate.

Two Y atoms configuration	*M* (*B*-site)	a. *E* ($Sr_{32}M_{30}Y_2O_{95}$)	b. E_M (H_2O)	c. *E* ($Sr_{32}M_{30}Y_2O_{96}H_2$)	d. c − (a + b)
Close	Ce	−1161.279	−14.22	−1176.278	−0.779
	Zr	−1315.586	−14.22	−1331.137	−1.331
Distant	Ce	−1160.195	−14.219	−1177.736	−3.322
	Zr	−1315.127	−14.22	−1330.3	−0.953

hydration is energetically favored in both the cerate and zirconate. In both the hydrated and dehydrated forms, as shown in Table 3, the enthalpy of the supercell with the Y atoms in close proximity was lower than that of the case wherein the Y atoms were further apart. This means that the cell configuration containing the Y atoms in close proximity was favored over the configuration wherein the Y atoms were further apart.

Chemical expansion due to hydration was evaluated by comparing the cell volumes of $Sr_{32}M_{30}Y_2O_{95}$ with those of $Sr_{32}M_{30}Y_2O_{96}H_2$ (M = Ce or Zr). The chemical expansion coefficient, β_{chem}, was calculated using the chemical expansion ratio ($\Delta V_{lattice}/V_{lattice}$) and protonic defect concentration ([OH]). As shown in Table 4, in the case of the Y atoms in close proximity, $Sr_{32}Ce_{30}Y_2O_{95}$ had a chemical expansion coefficient 1.6 times smaller than that of $Sr_{32}Zr_{30}Y_2O_{95}$. The experimentally determined chemical expansion coefficient of $SrCe_{0.922}Y_{0.078}O_{3-\delta}$ was larger than that of $SrZr_{0.922}Y_{0.078}O_{3-\delta}$, showing the opposite tendency. In contrast, in case of the Y atoms further apart, $Sr_{32}Ce_{30}Y_2O_{95}$ exhibited a chemical expansion coefficient 3.1 times larger than that of $Sr_{32}Zr_{30}Y_2O_{95}$, which is in agreement with the experimental results. As shown in Table 3, the cell was more energetically stable when the Y atoms were in close proximity than when they were further apart. If only the most stable atomic configuration is considered, the DFT calculations predict a smaller chemical expansion coefficient for the cerate than for the zirconate. However, considering the preparation process for these materials which involves sintering at high temperatures and successive cooling, along with the relatively low mobility of yttrium, it is reasonable that the material could exist in a mixture of the two different Y atom configurations. Omata et al. reported that both Y-O-Y and Y-O-Zr configurations coexist in Y-doped strontium zirconate, as determined by infrared spectroscopy [21]. Furthermore, Yugami et al. stated that increasing the Y concentration in Y-doped strontium cerates results in disorder of the Y distribution in the lattice [22]. These reports support the possibility of the mixed Y configuration.

Based on these results, the experimental observation that $SrCe_{0.922}Y_{0.078}O_{3-\delta}$ had a higher chemical expansion coefficient than $SrZr_{0.922}Y_{0.078}O_{3-\delta}$ can be accounted for by the DFT calculation. The chemical expansion coefficient of $Sr_{32}Ce_{30}Y_2O_{95}$ is lower than that of $Sr_{32}Zr_{30}Y_2O_{95}$ when the Y atoms are in close proximity, but higher when the Y atoms are far apart. Considering the sample preparation process and the previously mentioned studies, the two Y configurations were presumed to coexist, resulting in the higher chemical expansion coefficient for $SrCe_{0.922}Y_{0.078}O_{3-\delta}$ than $SrZr_{0.922}Y_{0.078}O_{3-\delta}$.

3.4. Oxide ion vacancy size in DFT-optimized geometry

To explain why the chemical expansion due to hydration depends on the configuration of the Y atoms, the sizes of the oxide ion vacancies in $Sr_{32}Ce_{30}Y_2O_{95}$ and $Sr_{32}Zr_{30}Y_2O_{95}$ were evaluated. During hydration, the oxide ion vacancies accommodate water molecules. Local stress originating from the incorporation of oxygen atoms into the vacancies, as well as the following relaxation, result in the chemical expansion. Thus, smaller oxide ion vacancies may possibly result in a larger degree of chemical expansion. Marrocchelli et al. investigated the chemical expansion of CeO_2- and ZrO_2-based fluorites by DFT and molecular dynamics calculation and showed that oxide ion vacancy is smaller than oxide ion so that the formation of oxide ion vacancy leads to the lattice contraction [24]. The result in the literature supports the assumption that filling of smaller oxide ion vacancy would result is large lattice expansion. Fig. 4 shows the results of evaluating the sizes of the oxide ion vacancies in $Sr_{32}Zr_{30}Y_2O_{95}$ and $Sr_{32}Ce_{30}Y_2O_{95}$, by use of the atomic coordinates determined by geometry optimization and Shannon's ionic radii [23]. As shown in Fig. 4(a1) and (b1), which correspond to the case wherein the Y atoms are in close proximity, the radius of the oxide ion vacancy in $Sr_{32}Ce_{30}Y_2O_{95}$ was 1.69 Å, which is larger than that in $Sr_{32}Zr_{30}Y_2O_{95}$, 1.30 Å. On the other hand, Fig. 4(a2) and (b2), which correspond to the case wherein the Y atoms were further apart, the radii of the oxide ion vacancies in $Sr_{32}Zr_{30}Y_2O_{95}$ and $Sr_{32}Ce_{30}Y_2O_{95}$ were both 1.24 Å. The observation that $Sr_{32}Ce_{30}Y_2O_{95}$ exhibited a lesser degree of chemical expansion than $Sr_{32}Zr_{30}Y_2O_{95}$ in the close-proximity Y configuration is explained by the larger oxide ion vacancy in the former. This feature can also be energetically explained. The magnitude of the negative enthalpy change originated from hydration (column d in Table 3) decreases with the size of oxide vacancy. This can be interpreted that the inducing local stress for the hydration is larger as the oxide ion vacancy is smaller. Hydration process is divided into the incorporation of oxygen into the oxide-ion vacancy and the introduction of hydrogen. The above discussion may reveal that the oxide ion vacancy is energetically more stable as the size of the vacancy becomes smaller. Although some other factors could influence the chemical expansion behavior, these results indicate a correlation between the chemical expansion and the size of the oxide ion vacancies to be hydrated. The result of a low chemical expansion in $Sr_{32}Ce_{30}Y_2O_{95}$ in the case of Y-Y close configuration is corresponded by the large size of oxide-ion vacancy. In other words, the chemical expansion is dependent on the Y configurations because the size of the oxide ion vacancy differs by the Y configurations.

Table 4
Chemical expansion of $Sr_{32}M_{30}Y_2O_{95}$ (M = Ce or Zr) by hydration process depending on Y configuration: The case that Y atoms are close each other and the case that Y atoms are distant each other.

Two Y atoms configuration	*M* (*B*-site)	$Sr_{32}M_{30}Y_2O_{95}$ (Å^3)	$Sr_{32}M_{30}Y_2O_{96}H_2$ (Å^3)	Chemical expansion	Chemical expansion Coefficient: β_{chem}
				$\Delta V_{lattice}/V_{lattice}$	$(\Delta V_{lattice}/V_{lattice})$ / [OH]
Close	Ce	2565.66	2570.5	0.0018	0.0288
	Zr	2280.73	2287.34	0.0028	0.0448
Distant	Ce	2546.88	2562.6	0.0061	0.0976
	Zr	2219.92	2224.41	0.002	0.032

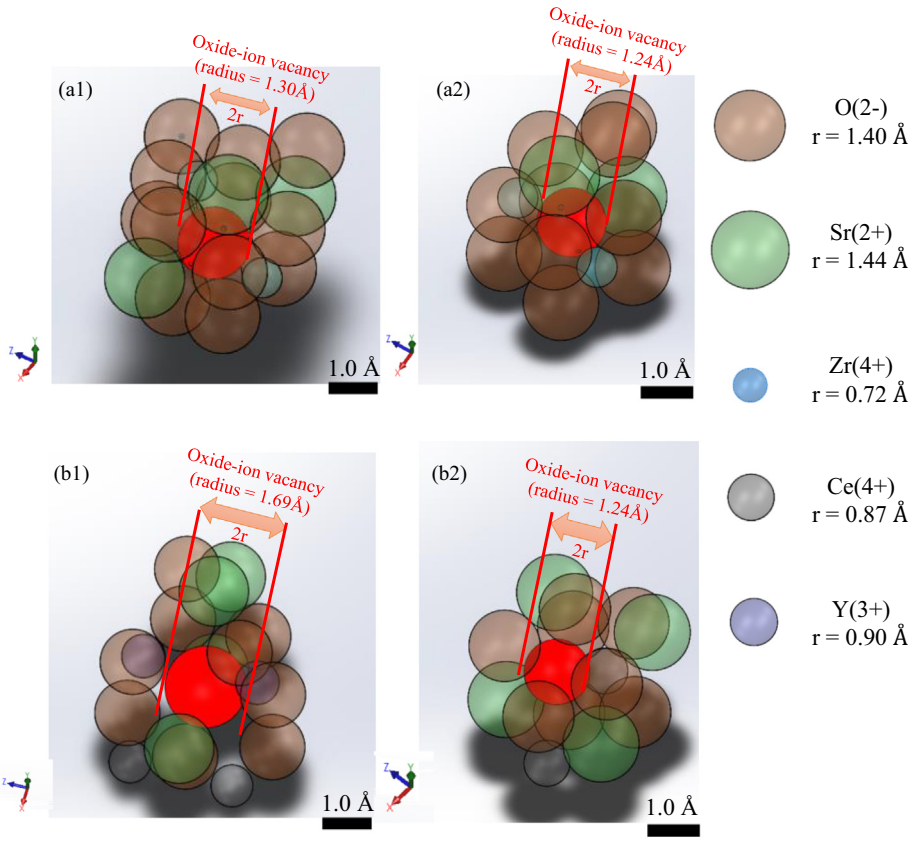

Fig. 4. (Color online) Oxygen vacancy sizes in $Sr_{32}Ce_{30}Y_2O_{95}$ and $Sr_{32}Zr_{30}Y_2O_{95}$ depending on Y configuration: Y atoms are close each other in $Sr_{32}Zr_{30}Y_2O_{96}H_2$ (a1), Y atoms are distant each other in $Sr_{32}Zr_{30}Y_2O_{96}H_2$ (a2), Y atoms are close each other in $Sr_{32}Ce_{30}Y_2O_{96}H_2$ (b1), and Y atoms are distant each other in $Sr_{32}Ce_{30}Y_2O_{96}H_2$ (b2). Orange, green, light blue, gray, and purple spheres are oxygen, strontium, zirconium, cerium, and yttrium, respectively. The sign of r means Shannon radii of respective atoms. (For interpretation of the references to color in this figure legend, the reader is referred to the web version of this article.)

3.5. Elastic character of $Sr_{32}Ce_{30}Y_2O_{95}$ and $Sr_{32}Zr_{30}Y_2O_{95}$

As mentioned previously, chemical expansion is considered to be the result of the relaxation of local stress due to the incorporation of oxide ions into vacancies. Thus, the elastic character of the material should also influence the chemical expansion; a lower bulk elastic modulus should give rise to a greater degree of chemical expansion. We investigated lattice enthalpy changes in $Sr_8Ce_6Y_2O_{23}$ and $Sr_8Zr_6Y_2O_{23}$ upon isotropic deformation between −2% and +2% by volume. Fig. 5 shows lattice enthalpy as a function of the isotropic deformation. The fitted line for $Sr_8Ce_6Y_2O_{23}$ exhibits a lesser degree of curvature than that of $Sr_8Zr_6Y_2O_{23}$, indicating that the cerate has a smaller bulk elastic modulus than the zirconate. This means that the cerate should undergo more extensive deformation than the zirconate in response to the same level of stress. This difference between the elastic moduli of the cerate and zirconate can explain the result shown in the former section for the configuration wherein the Y atoms were spaced further apart. Despite the similar sizes of the oxide ion vacancies as shown in Fig. 4(a2) and (b2), $Sr_{32}Ce_{30}Y_2O_{95}$ has a higher chemical expansion coefficient than $Sr_{32}Zr_{30}Y_2O_{95}$ (Table 4). This can be attributed to the lower elastic modulus of the cerate in comparison to that of the zirconate.

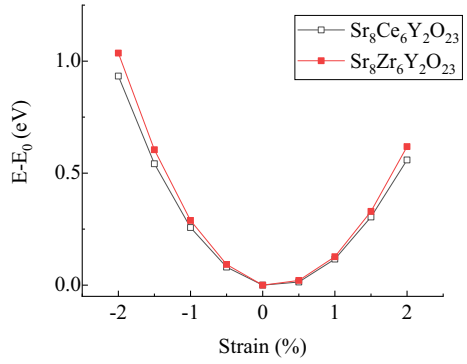

Fig. 5. Lattice energy comparison as a function of bulk modulus for $Sr_8M_6Y_2O_{23}$ (M = Ce or Zr). E_0 indicates the lattice energy of respective structure at 0% strain.

One possible explanation for the difference in the elastic modulus is the difference between the Ce—O and Zr—O bond lengths. Anderson and Soga reported that chemical bonds become weaker as bond length increases [25]. Because Ce is larger than Zr, the bulk modulus of cerate will be smaller than zirconate. Another possible explanation involves the ionicity/covalency of B—O bonds (B = Ce or Zr). Covalent bonds have relatively higher force constants than ionic bonds, and thus higher covalency may result in lower chemical expansion (and vice versa). To compare the iconicity/covalency of B—O bonds in the materials used in this study, the electron densities in $Sr_{32}Ce_{30}Y_2O_{95}$ and $Sr_{32}Zr_{30}Y_2O_{95}$ were mapped, as shown in Fig. 6(c) and (d), wherein the blue planes in Figs. 6(a) and (b) follow the center of one B-site and the nearest oxygen. As shown in Fig. 6(e), the electron density between Ce and O is lower than that between Zr and O. This means that the Ce—O bond has less covalent character than the Zr—O bond, which may explain the difference between the chemical expansion coefficients of $Sr_{32}Ce_{30}Y_2O_{95}$ and $Sr_{32}Zr_{30}Y_2O_{95}$.

The DFT calculation results indicated that the chemical expansion in $Sr_{32}Ce_{30}Y_2O_{95}$ and $Sr_{32}Zr_{30}Y_2O_{95}$ differs based on the configuration of the Y dopant atoms, as shown in Section 3.3. The results discussed in Sections 3.4 and 3.5 suggest correlations between the chemical expansion and differences in the size of oxygen vacancies and elastic moduli between the cerate and zirconate. The size of oxygen vacancies and the elastic modulus are thus the factors that explain the differences in chemical expansion behavior between the cerate and zirconate.

4. Conclusion

We investigated the effect of Ce and Zr in yttrium-doped strontium

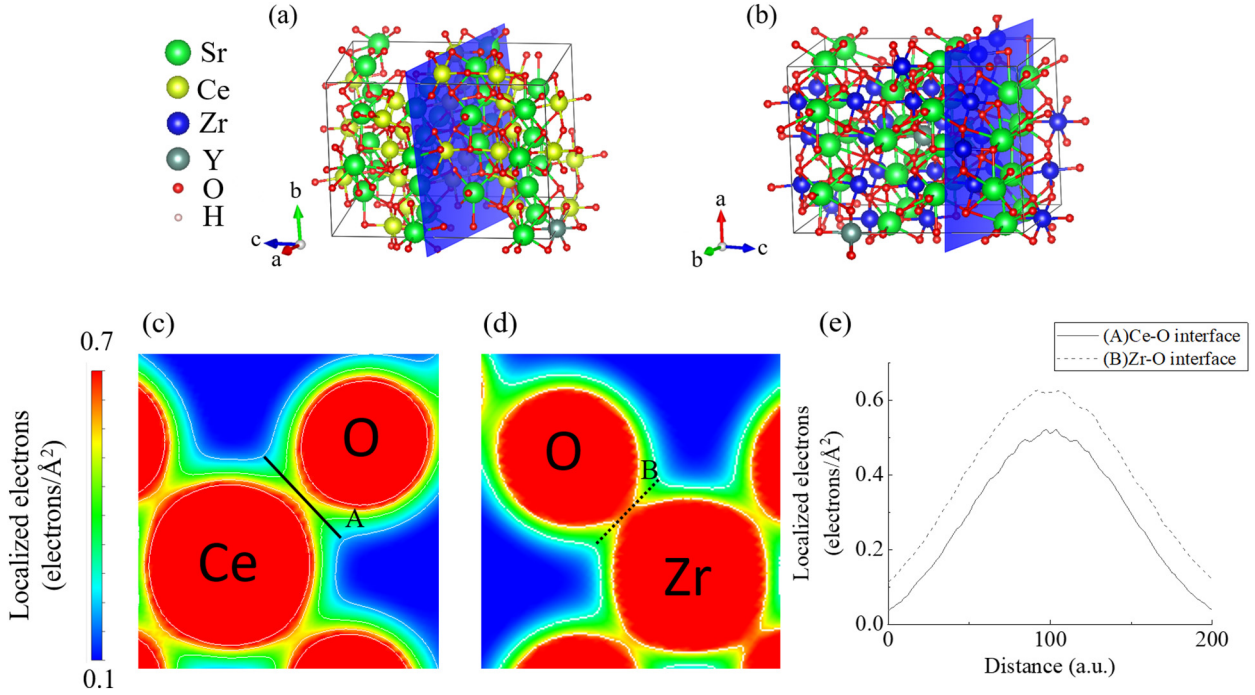

Fig. 6. (Color online) Electron density mapping planes (blue planes) in $Sr_{32}Ce_{30}Y_2O_{95}$ (a) and $Sr_{32}Zr_{30}Y_2O_{95}$ (b) in case that two Y atoms are distant each other. Miller indices for each plane are (−4.60637–1.00000 18.10390) in $Sr_{32}Ce_{30}Y_2O_{95}$ and (−5.41039 1.00000 34.8758) in $Sr_{32}Zr_{30}Y_2O_{95}$. Electron density maps at the interface between Ce/Zr and O: Ce—O interface in $Sr_{32}Ce_{30}Y_2O_{95}$ (c), Zr—O interface in $Sr_{32}Zr_{30}$ Y_2O_{95} (d) and localized electrons comparison with Ce—O (line A in panel e) and Zr—O (dotted line B in panel d) interface (e). (For interpretation of the references to color in this figure legend, the reader is referred to the web version of this article.)

zirconate and cerate on chemical expansion by hydration. HT-XRD and TGA indicated that the cerate has a chemical expansion coefficient approximately 4 times larger than that of the zirconate.

DFT calculations suggested that the chemical expansion coefficient is dependent on the configuration of the Y atoms; the cerate exhibited lower chemical expansion than the zirconate when the Y atoms were in close proximity and higher chemical expansion when the Y atoms were further apart. Thus, the experimental observation of the larger degree of chemical expansion in the cerate than in the zirconate can be attributed to the mixed presence of both configurations of Y atoms.

DFT calculations suggested that the size of oxide ion vacancies differs based on the Y atom configuration; when the Y atoms were in close proximity, the cerate exhibited larger oxide ion vacancies than the zirconate, which resulted in the lesser degree of chemical expansion in the former. The results indicated a correlation between the chemical expansion and the size of oxide ion vacancies to be hydrated, and that the size of the oxide ion vacancies is correlated with the configuration of Y dopant atoms. The elastic character is another factor influencing the different chemical expansion behavior of the cerate and zirconate; the former has a lower bulk elastic modulus which led to a higher degree of chemical expansion.

Acknowledgement

This project was supported by the Japan Society for the Promotion of Science (JSPS) and National Science Foundation (NSF) under the JSPS-NSF Partnerships for International Research and Education (PIRE), the JSPS Core-to-Core Program of Advanced Research Networks (Solid Oxide Interfaces for Faster Ion Transport), the International Institute for Carbon-Neutral Energy Research (I2CNER) of the World Premier International Research (WPI) in MEXT of Japan, and the Advanced Graduate Program in Global Strategy for Green Asia of Kyushu University.

Appendix A. Supplementary data

Supplementary data to this article can be found online at https://doi.org/10.1016/j.ssi.2019.01.009.

References

[1] S.H. Mohr, J. Wang, G. Ellem, J. Ward, D. Giurco, Fuel 141 (2015) 120–135, https://doi.org/10.1016/j.fuel.2014.10.030.
[2] P. Lianos, Appl. Catal. B Environ. 210 (2017) 235–254, https://doi.org/10.1016/j.apcatb.2017.03.067.
[3] M.S. Dresselhaus, I. Thomas, Nature 414 (2001) 332–337, https://doi.org/10.1038/35104599.
[4] K. Zagórski, S. Wachowski, D. Szymczewska, A. Mielewczyk-Gryń, P. Jasiński, M. Gazda, J. Power Sources 353 (2017) 230–236 (doi:10.1016%2Fj.jpowsour.2017.04.007).
[5] H. Matsumoto, T. Shimura, H. Iwahara, T. Higuchi, K. Yashiro, A. Kaimai, T. Kawada, J. Mizusaki, J. Alloys Compd. 408–412 (2006) 456–462, https://doi.org/10.1016/j.jallcom.2004.12.093.
[6] H. Iwahara, T. Esaka, H. Uchida, N. Maeda, Solid State Ionics 3–4 (1981) 359–363, https://doi.org/10.1016/0167-2738(81)90113-2.
[7] A.K.E. Andersson, S.M. Selbach, C.S. Knee, T. Grande, J. Am. Ceram. Soc. 97 (2014) 2654–2661, https://doi.org/10.1111/jace.12990.
[8] I.D. Seymour, a A. Chroneos, J.A. Kilner, R.W. Grimes, Phys. Chem. Chem. Phys. 13 (33) (2011) 15305–15310 https://doi.org/10.1039/C1CP21471C.
[9] D. Rupasov, A. Chroneos, D. Parfitt, J.A. Kilner, R.W. Grimes, S.Ya. Istomin, E.V. Antipov, Phys. Rev. B 79 (17) (2009) 172102, , https://doi.org/10.1103/PhysRevB.79.172102.
[10] Y. Jing, H. Matsumoto, N.R. Aluru, Mechanistic insights into hydration of solid oxides, Chem. Mater. 30 (2018) 138–144, https://doi.org/10.1021/acs.chemmater.7b03476.
[11] F. Krug, T. Schober, T. Springer, Solid State Ionics 81 (1995) 111–118, https://doi.org/10.1111/jace.12990.
[12] T. Schober, Solid State Ionics 145 (2001) 319–324, https://doi.org/10.1016/S0167-2738(01)00926-2.
[13] G. Kresse, J. Furthmüller, Phys. Rev. B 54 (1996) 11169–11186, https://doi.org/10.1103/PhysRevB.54.11169.
[14] G. Kresse, D. Joubert, Phys. Rev. B 59 (1999) 1758–1775, https://doi.org/10.1103/PhysRevB.59.1758.
[15] G. Kresse, J. Furthmüller, Comput. Mater. Sci. 6 (1996) 15–50, https://doi.org/10.1016/0927-0256(96)00008-0.
[16] J.P. Perdew, K. Burke, M. Ernzerhof, Phys. Rev. Lett. 77 (1996) 3865–3868, https://doi.org/10.1103/PhysRevLett.77.3865.

[17] Y. Chen, P. Hu, M.H. Lee, H. Wang, Surf. Sci. 602 (2008) 1736–1741, https://doi.org/10.1016/j.susc.2008.02.036.
[18] M.A. Gomez, S. Jindal, K.M. Fletcher, L.S. Foster, N.D.A. Addo, D. Valentin, C. Ghenoiu, A. Hamilton, J. Chem. Phys. 126 (2007) 194701, , https://doi.org/10.1063/1.2735592.
[19] A. Ahtee, M. Ahtee, A.M. Glazer, A.W. Hewat, Acta Crystallogr. B 32 (12) (1976) 3243–3246, https://doi.org/10.1107/S0567740876010029.
[20] M. Swift, C.G. Van de Walle, J. Phys. Chem. C 120 (2016) 9562–9568 https://pubs.acs.org/doi/10.1021/acs.jpcc.6b00765.
[21] T. Omata, Y. Noguchi, S. Otsuka-Yao-Matsuo, J. Electrochem. Soc. 152 (2005) E200–E205 https://pubs.acs.org/doi:10.1149/1.1899269.
[22] H. Yugami, Y. Chiba, M. Ishigame, Solid State Ionics 77 (1995) 201–206, https://doi.org/10.1016/0167-2738(94)00263-R.
[23] R.D. Shannon, Acta Crystallogr. 32 (1976) 751–767, https://doi.org/10.1107/S0567739476001551.
[24] D. Marrocchelli, S.R. Bishop, H.L. Tuller, B. Yildiz, Adv. Funct. Mater. 22 (2012) 1958–1965 https://pubs.acs.org/10.1002/adfm.201102648.
[25] O.L. Anderson, N. Soga, J. Geophys. Res. 72 (1967) 5754–5757, https://doi.org/10.1029/JZ072i022p05754.
[26] K. Momma, F. Izumi, J. Appl. Crystallogr. 44 (2011) 1272–1276, https://doi.org/10.1107/S0021889811038970.